공학석사 학위논문

High Energy Density Lithium Ion Hybrid Capacitor with Fast Kinetics of Expanded Graphite/Copper Oxide Composite Electrode

흑연/구리 산화물 전극을 이용한 고에너지 밀도 리튬 이온 커패시터

2019 년 2월

서울대학교 융합과학기술대학원

융합과학부 나노융합전공

이 성 훈

High Energy Density Lithium Ion Hybrid Capacitor with Fast Kinetics of Graphite/Copper Oxide Composite Electrode

지도교수 김연상

이 논문을 공학석사학위논문으로 제출함

2019 년 1월

서울대학교 융합과학기술대학원

융합과학부 나노융합전공

이 성 훈

이성훈의 석사학위논문을 인준함

2019 년 1월

위 원 장 박 원 철 (인)

부 위 원 장 김 연 상 (인)

위 원 유 지 영 (인)

Abstract

High Energy Density Lithium Ion Hybrid Capacitor with Fast Kinetics of Expanded Graphite/Copper Oxide Composite Electrode

Seong-Hun Lee

Program in Nano Science and Technology

Department of Transdisciplinary Studies

Graduate school of Convergence Science & Technology

Seoul National University

Recently high capacity energy storage devices are highlighted due to rapid growth of electric vehicles (EVs) and large-scale grid energy storage system. Especially Li ion batteries (LIBs) is the most suitable energy storage devices for EVs performing with high energy density. However, LIBs have some problems. The first is slow charging time issues owing to intrinsic reaction mechanism. The second is operating voltage range limit which is directly

connected to energy density derived from revisable capacity of cathodic material. The last is cost of cathode materials because of their scarcity. To overcome these issues, we introduce hybrid energy storage system that delivers high energy density without sacrificing power density. This hybrid system is made up of expanded graphite/copper oxide composite (GCuO) as the negative electrode and activated carbon (AC) as the positive electrode. The GCuO is high capacity materials by intercalation/deintercalation and conversion reaction. The AC provides large capacitance by ion adsorption/desorption. Additionally, both the active materials are abundant and low price. So, this system shows the three type of energy storage mechanism. The GCuO is synthesized by a simple process, through heat treatment of the Cu ion complex and pristine graphite. When the Cu ion complex is thermal decomposed, H_2 and CO_2 gases are generated. These gases induce the graphite planes expanded, the gap between the planes is increased from 0.34 nm to 0.39 nm. Also, copper oxide is in-situ formed on the graphite plane. The expanded graphite has a lower Li+ ion insertion barrier than the pristine graphite. So the synthesized material leads to a fast diffusion of Li ions on the negative electrode. As a result, a high power density can be obtained by enhanced charge transfer between the electrode and the electrolyte.

Before the full cell assembled, GCuO electrode needs to be pre-lithiation step under proper conditions since the positive electrode is not a lithium source

unlike the LIBs. The pre-lithiation is very effective for lowering the potential of the negative electrode and forming a stable SEI (Solid Electrolyte Interface) layer. Due to the lowered negative electrode potential, a full cell had a wide operating potential window, which can obtain a higher energy density. Optimized full cell shows high specific energy of about 250 Wh kg^{-1} at specific power of 250 W kg^{-1}, which is equivalent to LIB's energy density performance and the specific energy remain 70 Wh kg^{-1} when the specific power of 10 kW kg^{-1} within the voltage range of 1.0 V to 4.0 V.

Key words : Lithium ion capacitor, Graphite interlayer spacing, Lithium ion battery, Super capacitor, Electric double layer, pre-lithiation

Student Number : 2017-26520

Table of Contents

List of Figures

(b) GCuo8//AC and (c) GCuO4//AC full cells at different current density, (d) Three electrode full cell of GCuO4//AC with Li reference electrode at 0.1 A/g, (e) Cyclo-voltammogram of GCuO4//AC full cell at different scan rate, (f) cycle life of full cell at 100 mA g^{-1} voltage range from 1.0 V to 4.0 V.

Figure 3.11 (a) The galvanostatic charge-discharge curves of different GCuO//AC full cells with at 100mA g^{-1} and (b) Ragone plots for the GCuO//AC full cells , The GITT analysis and internal resistance during (c) discharging (d) charging of GCuOs half cell.

Figure 3.12 HR-TEM images of before pre-lithiation (a) Graphite, (c) GCuO4, (e) GCuO8, (g) GCuO16 and After pre-lithiation (b) Graphite, (d) GCuO4, (f) GCuO8, (h) GCuO16.

Figure 3.13 Repeated cyclo-voltammogram of (a) graphite, (b) GCuO4, (c) GCuO8 and (d) GCuO16 at 0.1 mV/s from 0.02 V to 2.5 V.

Figure 3.14. Nyquist plot analysis of GCuOs half cells from 0.1 Hz to 1 MHz.

List of Tables

Chapter 1. Introduction

1.1 Current energy storage device issue

Since the 19th century when fossil fuels began to be used, the temperature of the earth has increased every year. Fossil fuels led to global warming and the world average surface temperature rose by nearly 0.6 °C from 1906 to 2005. In the summer of 2018, the earth suffered from abnormal high temperatures. Consequently, climate change is expected to reduce the ecosystem diversity and cause many species to become extinct [1, 2]. To solve the global warming problem, we have to refrain from using fossil fuels, which are the main cause of greenhouse gases. As a result, considerable efforts have been made to research and commercialize alternative energies that do not use fossil fuels like solar power and wind power. In addition, transportation has been changed from internal combustion engine automobiles to electric vehicles (EVs) [3-5]. In both of these representative cases, stable energy storage devices are required. Because alternative energy has intermittent development, additional energy storage devices are needed and EVs require energy storage devices as an energy source. Li ion batteries (LIBs) are the most suitable energy storage devices for EVs performing with high energy densities [6]. However, EVs that used LIBs as energy sources have problems with slow charging and mileage.

1.2 Introduction to Lithium Ion Hybrid Capacitor

These issues have led to the development of power systems with high specific capacity LIBs. At the same time, these advanced batteries have solved the mileage and cost issues considerably. However, LIBs have intrinsic reaction mechanisms that induce slow charging times. Thus, a lithium ion hybrid capacitor (LIC) is being proposed to solve this problem as it employs a faradaic Li –intercalating electrode and a non-faradaic ion adsorption/desorption electrode. The hybrid of the two electrodes makes LIC have a power density higher than LIB and a higher energy density than Super Capacitors (SCs), especially electric double layer capacitors (EDLCs). The LIC is expected to bridge the gap between the LIBs and EDLCs and become the ultimate power source for hybrid electric vehicles (HEV) and EVs in the near future [7]. Therefore, many studies have been carried out recently as LICs are commonly composed of LIB anodes and SC cathodes to take advantage of the energy density and power density. For this reason, studies about anode materials have been studied in depth. 1) Studies about graphite, which is a conventional LIBs anode using organic electrolytes (graphite//activated carbon (AC)), started at the early stages. This hybrid system can operate high currents with moderate specific capacity and good stability [8, 9]. 2) Research using metal oxide & graphene composites. Graphene can improve the slow charge transfer reaction of the negative electrode (N-doped CNS //ZnMn2O4-rGO, PHPNC // TiC-rGO, a-TEGO//SnO2-rGO) [10-12]. On the other hand, when Si/Cu nanowires (NWs)

and AC are employed, it is possible to operate at high power densities to obtain high specific capacities [13]. However, the process goes through several steps and is complex and costly.

1.3 Lithium Ion Capacitor with GCuOs//AC

To overcome these issues, we designed a device that performs excellently through a simple process. The proposed hybrid system (LIC) is made up of expanded graphite/copper oxide composite (GCuO) as the negative electrode and activated carbon (AC) as the positive electrode. This system is schematically illustrated in Fig 1.1. The GCuO was synthesized by a simple process through heat treatment of the Cu ion complex and pristine graphite [14-16]. While the Cu ion complex is thermally decomposed, H_2 and CO_2 gases are generated and induce the graphite interlayer spacing to expand. The expanded graphite has a lower Li ion intercalation barrier than pristine graphite [17]. Therefore, the synthesized material enhances the charge transfer between the electrode and the electrolyte. The copper oxide on the graphite plane is a high specific capacity anode, which provides additional specific capacity (674 mAh g^{-1}, $CuO + 2Li^{+}+2e^{-} \leftrightarrow Li_2O + Cu$) [18]. The AC has a high specific surface area, which provides large capacitance by the ion adsorption/desorption [19]. Additionally, both the active materials are abundant and low in price, so this system can deliver a high energy density without sacrificing power density.

Combining two high specific capacity electrodes is not enough for a good

performance LIC. Since the reaction mechanisms of the two electrodes are different, it is necessary to balance the reaction kinetics. We derive the optimum electrode for LIC by the CuO/graphite ratio and electrode mass balance. If GCuO contains a large amount of CuO, a high specific capacity can be obtained by the conversion reaction of CuO. However, as the amount of copper oxide increases, the internal resistance of electrode also increases and degrades the LIC performance in terms of the power density and life span [16]. Before the full cell is assembled, the GCuO electrode needs to undergo a pre-lithiation step under proper conditions since the positive electrode does not have a Li ion source unlike the LIBs. Furthermore, the pre-lithiation process is very effective for lowering the negative electrode potential and forming a stable SEI (Solid Electrolyte Interface) layer [20]. Due to the lowered anode potential, the full cell has a wide operating potential window, which can obtain a higher energy density. In addition, the cycling characteristics of the prepared cell were also enhanced by preventing additional Li ion loss for forming a SEI layer [21, 22]. Finally, optimized full cells showed high specific energy of about 250 Wh kg-1 within the voltage range of 1.0~4.0V, which is equivalent to LIB's energy density performance. The manufactured full cell maintained an energy density of 70 Wh kg^{-1} even at a high power density of 12.5 kW kg^{-1} and the optimized full cell showed excellent energy efficiency over 95%, which is better than LIBs with 80%.

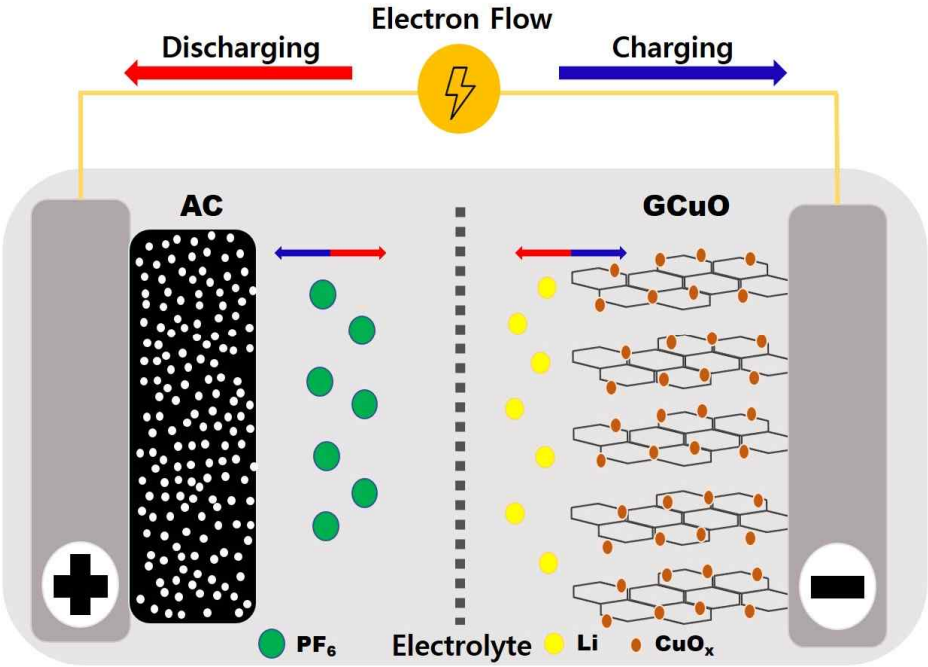

Figure 1.1 Schematic mechanism of the GCuO//AC hybrid systems.

Chapter 2. Experiments

2.1 Synthesis of Cu ion complex

The Cu ion complex was synthesized as follows. Amino-Methyl-Propanol (8.98 g) and octylamine (11.45 g) were mixed for 30 min in a 250 mL round-bottomed flask. Then, methyl alcohol (20 mL) and Cu (II) formate tetrahydrate (20 g) were added to the mixture. The color of the solution changed immediately to a permeable blue as soon as the Cu (II) formate tetrahydrate was poured in. The mixture was stirred for 1 h at room temperature. The solvent was removed under reduced pressure at 50 ℃ using a rotary evaporator. Then, the product was dried under vacuum for 8 hr at 50 ℃. The dry product was obtained as a dark blue, highly viscous complex. For control of the viscosity, the Cu ion complex and Isopropyl alcohol (IPA) were mixed in a 1 : 9 (w/w) ratio through sonication and vortex mixing [14, 15].

2.2 Fabrication of novel graphite/copper oxide (GCuOs)

The GCuO samples were fabricated by mixing pristine graphite and the IPA solution of the Cu ion complex in weight ratio of 1 : 4, 1 : 8, and 1 : 16 with a homogenizer (AR 100, Thinky mixer) at 1000rpm for 10 min. These were named GCuO4, GCuO8 and GCuO16. Each mixture was sintered at 350 ℃ for 4 hr in air condition [16].

2.3 Fabrication of cell

For electrode fabrication, a GCuO slurry was prepared by mixing a 6:3:1 weight ratio of GCuO, conductive carbon (Super P, Timcal) as conducting agent, and styrene butadiene rubber/carboxymethyl cellulose (SBR/CMC). Graphite were prepared using the same proportions for comparison. Activated carbon (CEP21KS, Power carbon technology) slurry was prepared by mixing AC, Super P, SBR/CMC at the weight ratio of with 85:10:5, respectively. The GCuO, graphite slurries were coated onto copper foil (9 mm thick, MTI korea), the AC slurry was coated onto aluminum foil (13 mm thick, KJCC) using a Meyer rod. The electrodes were dried at 120 ℃ and assembled into CR2032 coin cells. The half-cells were assembeld of a working electrode (GCuO, Graphite, AC), a separator (PP monolayer membrane: Celgard 2500), electrolyte (1M Lithium hexafluorophosphate ($LiPF_6$) in Ethyl carbonate (EC) / Dimethyl carbonate (DMC) / Diethyl carbonate (DEC) in the volume ratio 1:1:1), and a reference electrode (Li foil; thickness: 150 μm) under argon atmosphere.

The hybrid cell consists of pre-lithiated GCuO (4cycle at 0.1C, to 0.04V) as negative electrode and AC as positive electrode under argon atmosphere,. The mass ratio AC to GCuO is 3.5 ~ 4. The separator and electrolyte are same as used in half cell.

2.4 Material characterization

The GCuO were characterized by X-ray diffraction (XRD), Raman spectroscopy, transmission electron microscopy (TEM) ,and energy-dispersive

X-ray spectroscopy (EDS). XRD patterns and Raman spectrum were obtained by SmartLab (Rigaku) and DXR2xi (Thermo). TEM images and Energy Dispersive Spectroscopy (EDS) image were prepared with a JEM-2100F (JEOL) at 200 keV.

2.5 Electrochemical methods

All of the electrochemical tests were performed at ambient condition. Galvanostatic charge-discharge and GITT (Galvanostatic Intermittent Titration Technique) were studied using battery cycler (WBCS 3000L, WonATech). Cyclo-Voltammetry (CV), Electrochemical Impedance spectroscopy (EIS) and Galvanostatic charge-discharge were conducted using electrochemical workstation (VSP, BioLogic Science Instruments) with three electrode method. The specific energy density (**E**) and power density (**P**) were calculated from Galvanostatic charge-discharge curves by using the following formula. The mass used in the calculation was active materials from the positive and negative electrodes.

$$\mathbf{E} = \frac{\boldsymbol{i}}{\boldsymbol{m}} \int_{t_1}^{t_2} \boldsymbol{V dt} \qquad (\mathbf{1})$$

$$\mathbf{P} = \frac{\mathbf{E}}{\mathbf{t}} \qquad (\mathbf{2})$$

Where **i** is the discharge current (A), **V** is the discharge voltage (V), **t** is the discharge time (h) and **m** is the total mass of active materials from the positive and negative electrodes (kg).

Chapter 3. Result and Discussion

3.1 Material characteristics of GCuOs

Figure 3.1 showed the schematic mechanism of prepared GCuO obtained from the Cu ion complex ink through pyrolysis in air conditions. This pyrolysis generates hydrogen, carbon monoxide, carbon dioxide, and copper oxide. The generated gases widen the graphite layer gap, which is helpful in reducing Li ion insertion stress during charging. The decrement of insertion stress increases capacity and reduces internal resistance [16,17]. The Cu ion complex changes into the CuO nanoparticle through pyrolysis since it is very effective at enhancing specific capacity due to high theoretical capacity.

XRD analysis was carried out to confirm the synthesized copper oxide on graphite. Raman and TEM analyses were conducted to investigate the existence of expanded graphite. The XRD pattern of the graphite sample showed a typical graphite peak (JCPDS No. 41-1487). Cu oxide samples showed Cu (I) oxide (JCPDS No. 05-0667), Cu (II) oxide (JCPDS No. 41-0254), and Cu (JCPDS 04-0836) peaks [23-25]. The XRD data of the GCuO sample confirmed all of the aforementioned peaks (Fig. 3.2a). In the raman spectroscopy of the graphite, GCuO4, and GCuO16 samples, two dominant peaks were observed from graphite (Fig. 3.2b). The G band (1570 cm^{-1}) appears as the in-plane vibration of sp^2 carbon atoms and the relative degree of sample graphitization. The D band (1345 cm^{-1}) shows the presence of sp^3 carbon atoms or defective sites in

graphene [26]. Therefore, the existence of expanded graphite can be determined by the peak ratios of the G band and D band obtained from Raman analysis results. The I_d / I_g ratio values were increased by 0.24 for graphite, 0.70 for GCuO4, and 0.79 for GCuO16 (Fig. 3.2b). Therefore, the expansion ratio of graphite increases as the ratio of copper ion complex increases. Additionally, the positive shift of the G band (about 15 cm^{-1}) showed that carbon and copper are bonded together [27]. TEM was performed to directly detect the presence of expanded graphite by Raman analysis with an interlayer spacing of 0.34 nm. In the case of GCuO16, the spacing was 0.39 nm (Fig. 3.2c, d). GCuO4 and GCuO8 had interlayer spacings of approximately 0.36nm and 0.37nm (Fig. 3.3a, b). Increases in the interlayer spacing are induced by the gas produced from the copper ion complex thermal decomposition. The GCuO, which has a large amount of copper ion complex, has a wider interlayer spacing. The GCuO16 analysis by EDS also showed the existence of carbon, copper and oxygen (Fig. 3.4). Nitrogen adsorption/desorption analysis suggested that the specific surface area (SSA) of GCuO16, GCuO8, and GCuO4 were 4.69 m^2 g^{-1}, 4.22 m^2 g^{-1}, and 4.09 m^2 g^{-1}, respectively. These SSA value are larger than the graphite SSA of 2.98 m^2 g^{-1} due to the increase in the amount of copper oxide particles on graphite and extended (Fig. 3.5, Table 3.1).

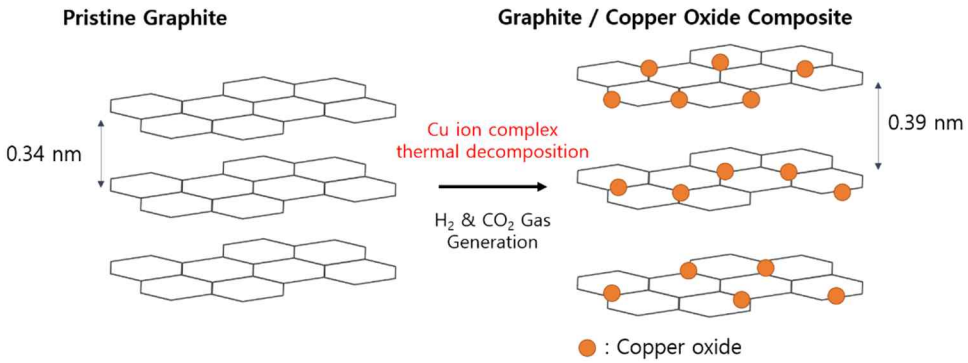

Figure 3.1 Schematic mechanism of graphite/copper oxide composite synthesis process. Thermal decomposition of Cu ion complex generates H_2 and CO_2 gases, which induce the graphite interlayer spacing expanded.

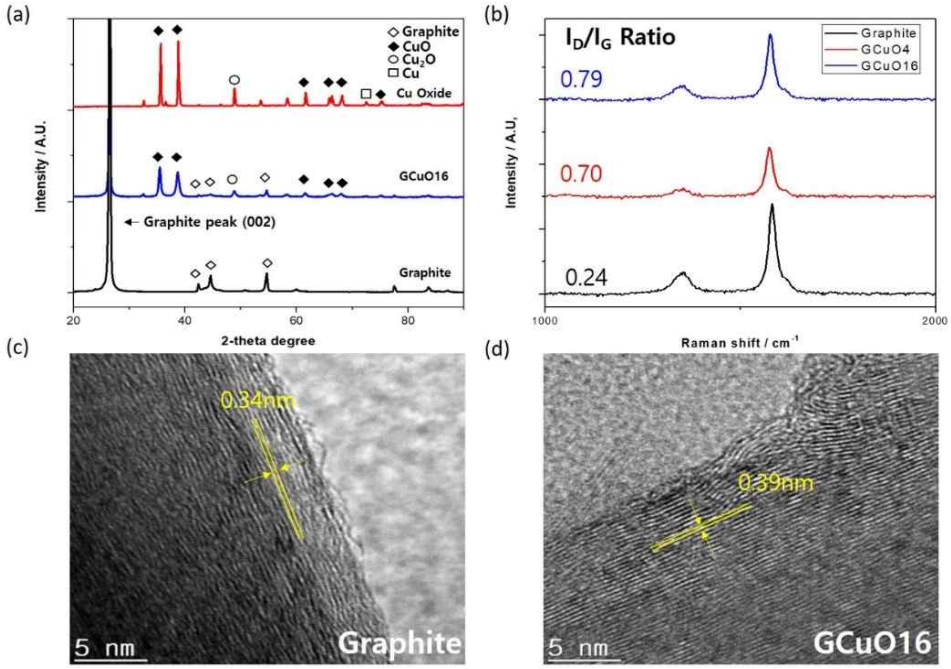

Figure 3.2 Charactreristics of fabricated materials : (a) XRD pattern of Cu Oxide, GCuO16 and graphtie (b) Raman spectra of GCuO and graphite D and G peaks, HR-TEM images of (c) Graphite, (d) GCuO16.

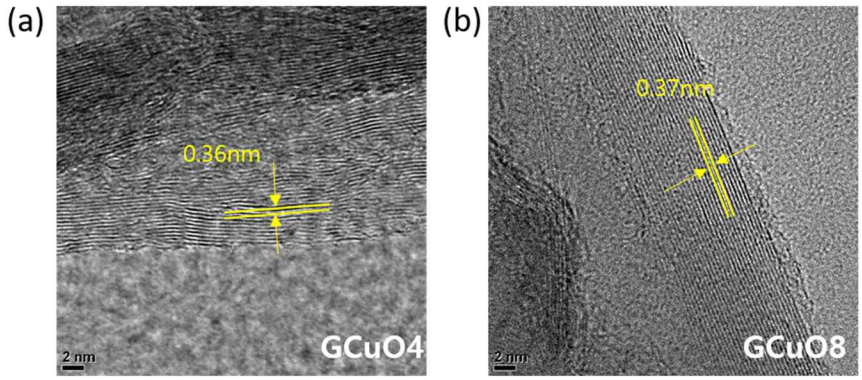

Figure 3.3 HR-TEM images of (a) GCuO4, (b) GCuO8.

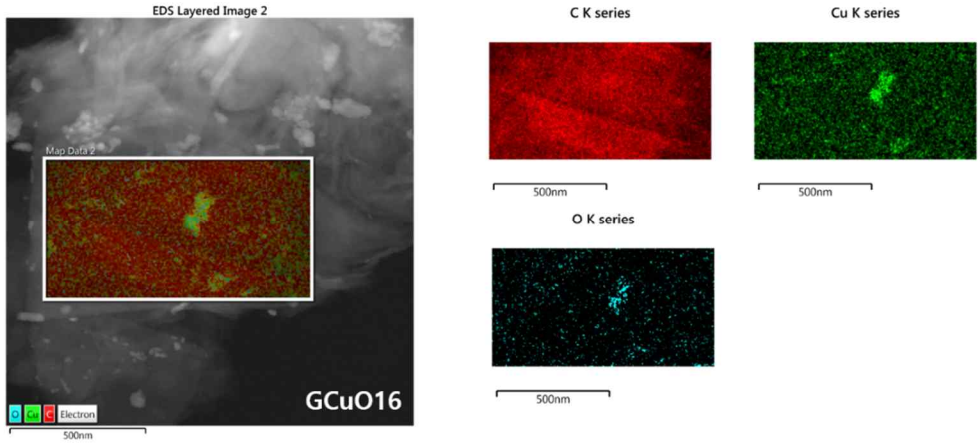

Figure 3.4 Energy Dispersive Spectroscopy (EDS) of GCuO16.

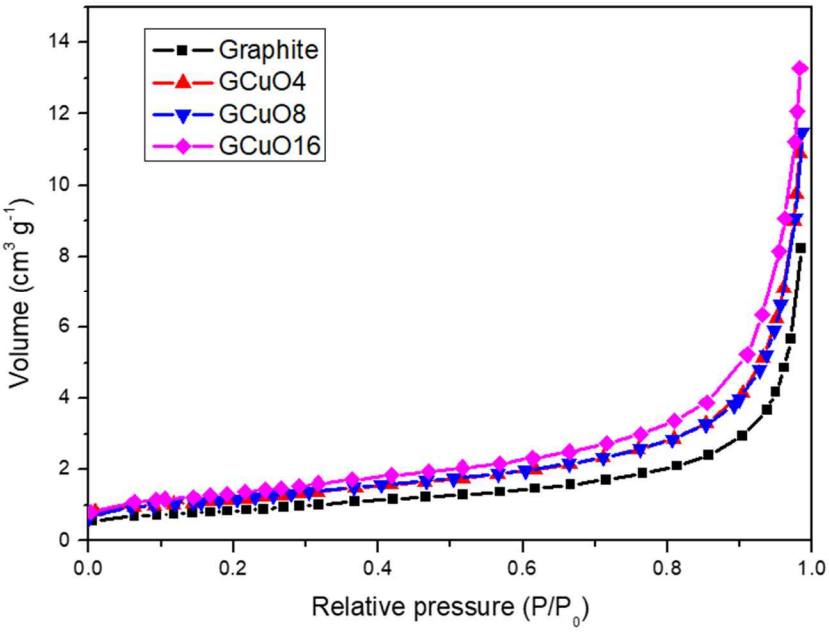

Figure 3.5 Nitrogen adsorption/desorption isotherms of GCuO4, GCuO8 and GCuO16.

Table. 3.1 Specific surface area (BET) of Graphite, GCuO4, GCuO8 and GCuO16.

	Graphite	GCuO4	GCuO8	GCuO16
BET ($m^2 g^{-1}$)	2.98	4.09	4.22	4.69

3.2 Electrochemical Performance of GCuOs and AC electrode

The electrochemical performance of the GCuOs and AC materials was investigated by the Li half cell system before full cell assembly. The galvanostatic charge-discharge curves of the GCuOs half cell were obtained by using GCuOs as working electrode and lithium metal as counter and reference electrodes in a voltage range from 0.02 to 2.5V. Figure 4.1a showed that as the amount of copper oxide increases in GCuO, the peak induced from the conversion reaction of copper oxide increases at 0.8V and 1.4 V [28]. The plateau ranges of intercalation/de-intercalation of Li ion to graphite can be observed under 0.2 V (Fig. 3.6a). Furthermore, the cyclo-voltammogram of GCuO4 half cell supports the results. 0.8 V and 1.4 V of cathodic peaks from the conversion reaction of copper oxide and under 0.2 V of cathodic peak from the intercalation of graphite were confirmed through CV data (Fig. 3.6b). The GCuO16 half cell (568 mAh g^{-1}) had higher specific capacity than the GCuO4 half cell (489 mAh g^{-1}) due to the higher copper oxide content. This specific capacity is similar regardless of low C-rate (0.2 C) or high C-rate (10 C) due to high theoretical capacity of copper oxide and low Li ion insertion barrier by the expanded interlayer spacing (Fig. 3.6c). The cyclo-voltammograms of the AC half cell were described in Fig. 3.7. In the range of 2.0 V to 4.0 V, the voltammogram showed a rectangular shape. This means there were no significant redox peaks in the AC electrode, showing that the capacitance of the

AC half cell mainly depends on a non-faradaic reaction induced ion adsorption/desorption. The galvanostatic charge-discharge profiles of the AC half cell correspond with the cyclo-voltammogram. These profiles showed an isometric triangular shape by a non-faradaic reaction in the voltage range of 2.0 to 4.0 at different current densities (Fig. 3.6d).

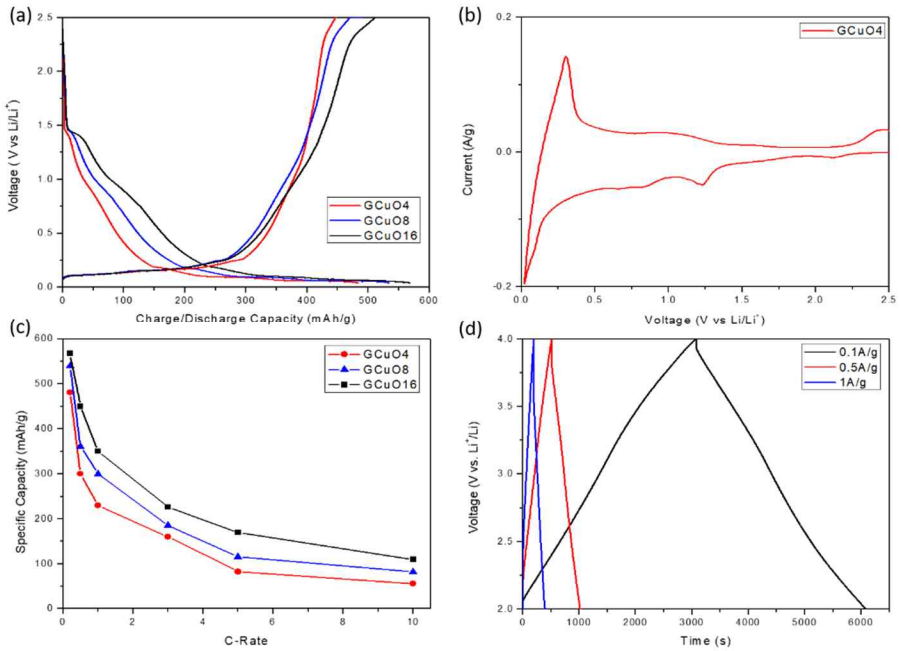

Figure 3.6 (a) The Galvanostatic charge-discharge curves at 0.2 C and (b) rate capability of GCuOs half cell in differenet C-rate, (c) Cyclo-voltammogram with 0.1 mV/s of GCuO4 half cell and (d) Galvanostatic charge-discharge with different current density of AC half cell.

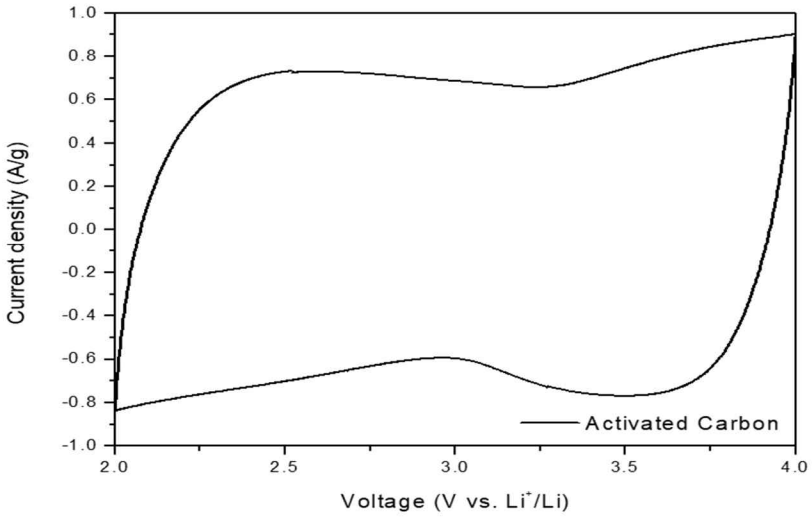

Figure 3.7 Cyclo-voltammogram with 10 mV/s of AC.

3.3 Electrochemical performance of the hybrid cell GCuOs//AC

Before hybrid full cell which is consist of GCuOs anode and AC cathode was assembled. GCuOs electrode was pre-lithiated for 4 cycle at 0.1C with Li metal to supplying Li source, forming stable SEI layer and expanding graphite inter-spacing. The mass ratio of AC to GCuOs was 3.5 ~ 4 for the charge balance between the cathode and the anode. The optimal voltage range was found through a three-electrode test. The experiment was conducted in the range of 2 ~ 4 V, 1 ~ 4 V and 0 ~ 4 V. The shortest voltage range (2 ~ 4 V) had the lowest specific capacity because copper oxide reaction is not occurred sufficiently in this voltage range (Fig. 3.8a). On the contrary, the widest voltage range (0 ~ 4 V) had the highest specific capacity (Fig. 3.8c), however specific capacity was faded to the 72% level comparing with initial specific capacity after 10^{th} cycles and this cell failure continuously proceed, only 56% of specific capacity was remained after 100^{th} cycles. That is due to excessive using conversion reaction of copper oxide (Fig. 3.8). The copper oxide undergoes a large volume change during charging-discharging process by conversion reaction, which induces hybrid cell capacity degradation [29]. Thus, 1 ~ 4 V range was specified as an appropriate range. GCuOs//AC full cells had high specific capacity and maintained 75% of initial specific capacity in 100^{th} cycle at the range of 1 ~ 4 V (Fig. 3.8b, 3.9). The galvanostatic charge-discharge curves of GCuOs//AC full cells showed the symmetric triangular shape with little hump in a potential

range of 1.0-4.0 V at a different current density (Fig. 3.10a-c). The hump is caused by conversion reaction of copper oxide (Fig. 3.10d). The hybrid cells can be operated at high current density of 5000 mA g^{-1}, which is difficult to apply on the conventional rechargeable batteries because of their intrinsic reaction on electrode. At low current densities, hybrid cell using GCuO4 have the highest energy density of 250 Wh kg^{-1}. Cyclo-voltammograms showed stable quasi - rectangular shaped curves with increasing scan rate, which is induced the difference storage kinetics between faradaic and non-faradaic reaction (Fig. 3.10e) [12]. At the 5 mV/s, 1.8 V and 2.5 V of anodic peaks are induced by conversion reaction of copper oxide and intercalation of graphite, respectively. The hybrid cell with GCuO4 maintains 82% of the initial energy density after 500 cycles. At this time, it has high energy efficiency over 95% compared to low energy efficiency of LIBs (Fig. 3.10f) [17]. The energy density gradually decreases inevitably, due to the volume change of copper oxide conversion reaction [29].

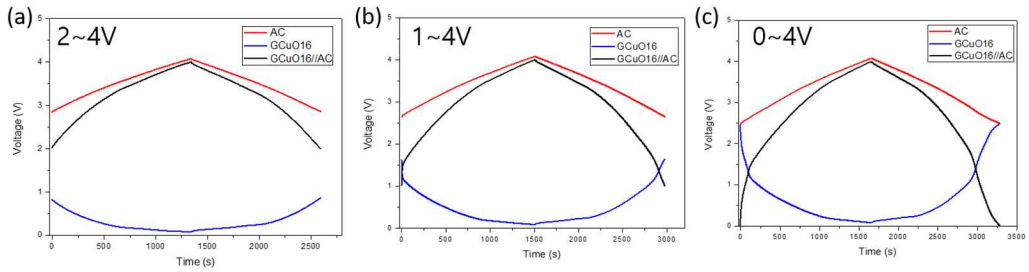

Figure 3.8 Three electrode full cell of GCuO16//AC with Li reference electrode at different voltage range (a) 2 – 4 V, (b) 1 -4 V, (c) 0 – 4 V.

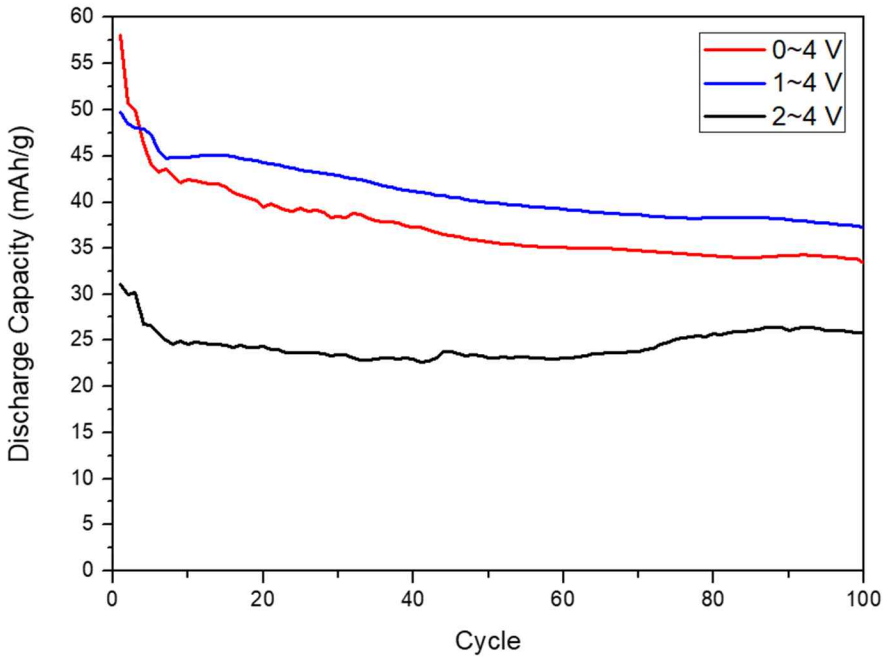

Figure 3.9 Cycle life of full cell at 100mA/g at different voltage range.

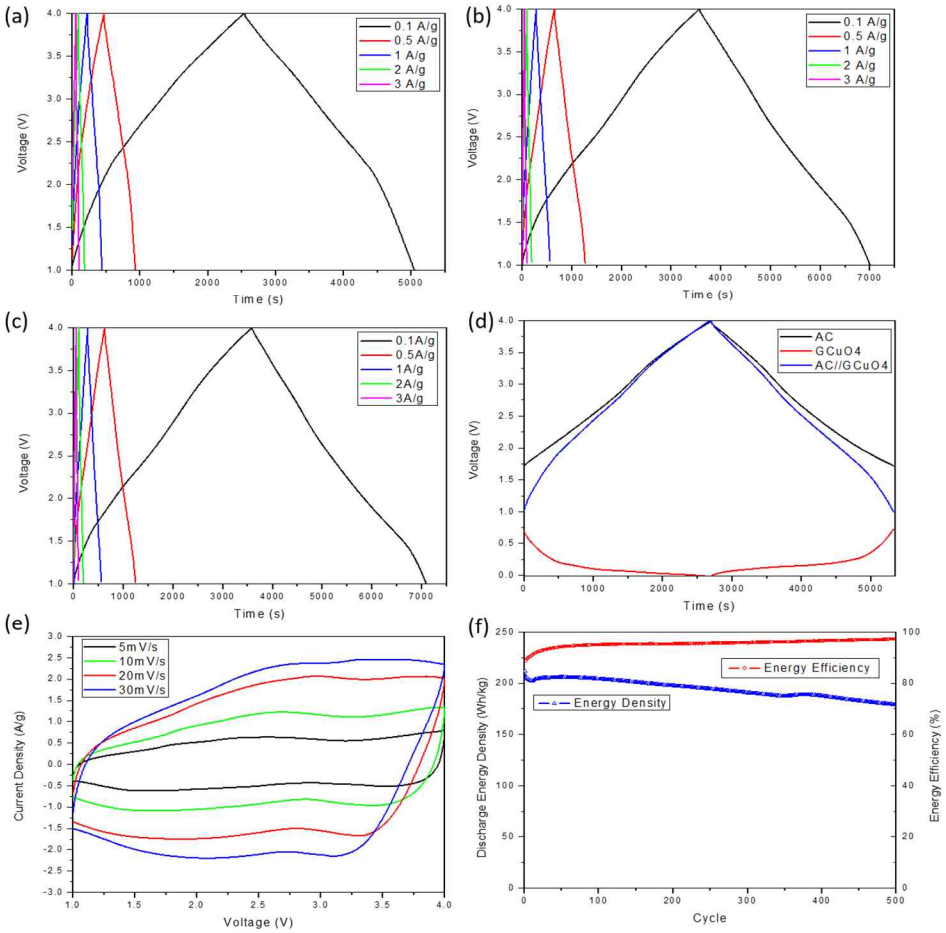

Figrue 3.10 The Galvanostatic charge-discharge curves of (a) GCuO16//AC, (b) GCuo8//AC and (c) GCuO4//AC full cells at different current density, (d) Three electrode full cell of GCuO4//AC with Li reference electrode at 0.1 A/g, (e) Cyclo-voltammogram of GCuO4//AC full cell at different scan rate, (f) cycle life of full cell at 100 mA g^{-1} voltage range from 1.0 V to 4.0 V.

3.4 Internal Resistance and Pre-lithiation effect

The energy densities of the GCuO4 and GCuO8 hybrid system were 250 Wh kg^{-1} and 246 Wh kg^{-1}, respectively. The GCuO4 and GCuO8 full cells showed higher energy density than the GCuO16 full cell at a low power density (Fig. 3.11a, b). The reasons for the energy density difference are internal resistance derived from the intrinsic resistance of copper oxide and pre-lithiation effect of graphite. In the case of a hybrid cell, the negative electrode has slower kinetics than the positive electrode, because the positive electrode stores the charge through ion adsorption/desorption. However, the negative electrode uses intercalation and conversion reaction [12]. Therefore, the negative electrode with lower internal resistance enhances the reaction rate and shows better performance within a hybrid cell; thus, balancing the fast kinetics of the positive electrode. The weight fractions of copper oxide of GCuO4, 8 and 16 are 7.8, 14.5 and 25.3 %, respectively (Table 3.3) [16]. As the amount of copper oxide increases, the internal resistance of the material also increases [30]. Because the copper oxide is not conductive, the full cell performance is reduced. This can be confirmed by using the Galvanostatic Intermittent Titration Technique (GITT) at the 1 C rate [30-32]. This technique measures the change in open-circuit voltage by cutting off the current supply during charging and discharging using a constant current. The internal resistance were proportional to the voltage change under a constant current. The value of internal resistance was obtained by dividing the voltage change by the applying current. At the

discharge depth of 20 to 60 %, the GCuO16 has over 60 Ω of internal resistance. On the other hand, the GCuO4 and 8 half cells have under 40 Ω of internal resistance (Fig. 3.11c). This same tendency is shown when charging GCuOs half cells (Fig. 3.11d). Therefore, the internal resistance of GCuO4 and 8 half cells are lower than GCuO16 half cell during charging and discharging. Additionally, the pre-lithiation also influences GCuO kinetics by increasing the interlayer spacing of GCuO4,8 at a similar interlayer spacing value of pre-lithiated GCuO16 (Fig. 3.12a-h). After pre-lithiation, the graphitic spacing of GCuO4, 8, and 16 after pre-lithiation are 0.42, 0.435, and 0.44 nm, respectively. Meanwhile, the graphite sample has interlayer spacing of 0.36 nm after pre-lithiation (Table 3.2). The expansion of the interlayer spacing GCuOs induced charging-discharging can be confirmed by repeated cyclo-voltammetry using GCuOs half cells. As the cycle progresses, GCuO4, 8, and 16 half cells increased the anodic peak by intercalation in graphite under 0.2 V, unlike the graphite half cell (Fig. 3.13a-d). These results imply that more Li ions are inserted into the graphite than before. Accordingly, GCuOs after pre-lithiation have wider interlayer spacing. Enlarging the graphitic spacing reduced the physical barrier of solvated Li ion insertion, so the internal resistance of cells decreased. The solvated Li ion insertion stress of GCuO4 and 8 is alleviated as much as GCuO16. Furthermore, the GCuO4 and GCuO8 hybrid cells have better energy densities than the GCuO16 hybrid cell at low power densities in the Ragone plot (Fig. 3.11b). Among them, the GCuO4 has the lowest intrinsic

resistance as shown in electrochemical impedance spectroscopy (EIS) results in Fig. 3.14. Consequently, chemical kinetics between AC and GCuO4 are balanced, so the GCuO4 was the most suitable negative electrode material in terms of energy density and power density as described in Fig. 4b. Based on these results, it is more important to balance the kinetics between the negative and positive electrodes, although a high specific capacity of negative electrode materials is also important in a hybrid system.

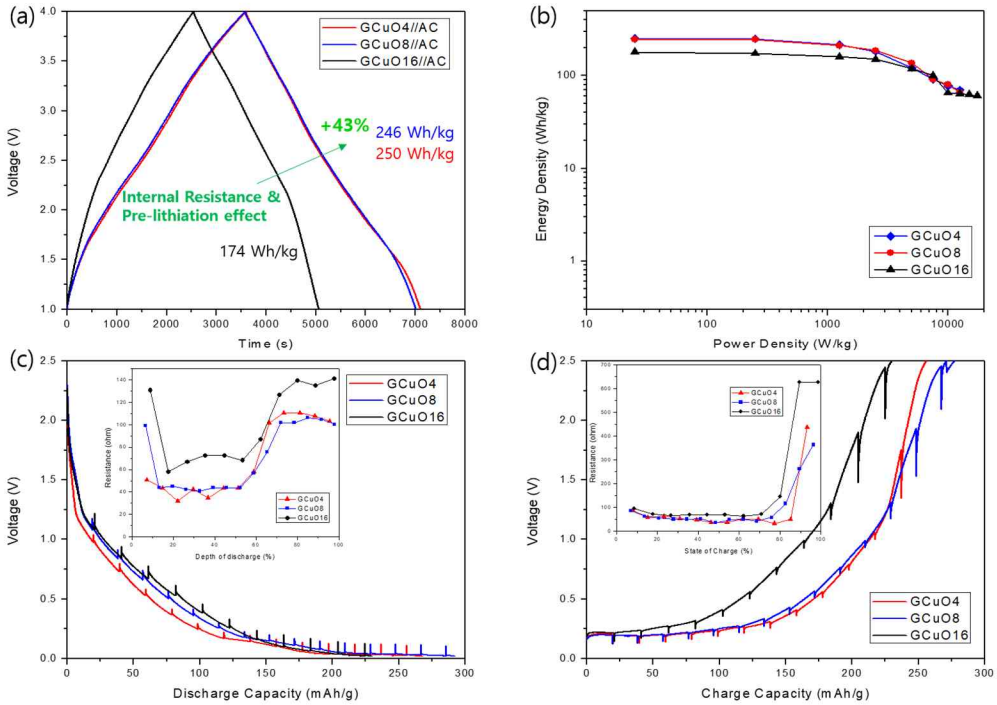

Figure 3.11 (a) The galvanostatic charge-discharge curves of different GCuO//AC full cells with at 100 mA g^{-1} and (b) Ragone plots for the GCuO//AC full cells , The GITT analysis and internal resistance during (c) discharging (d) charging of GCuOs half cell.

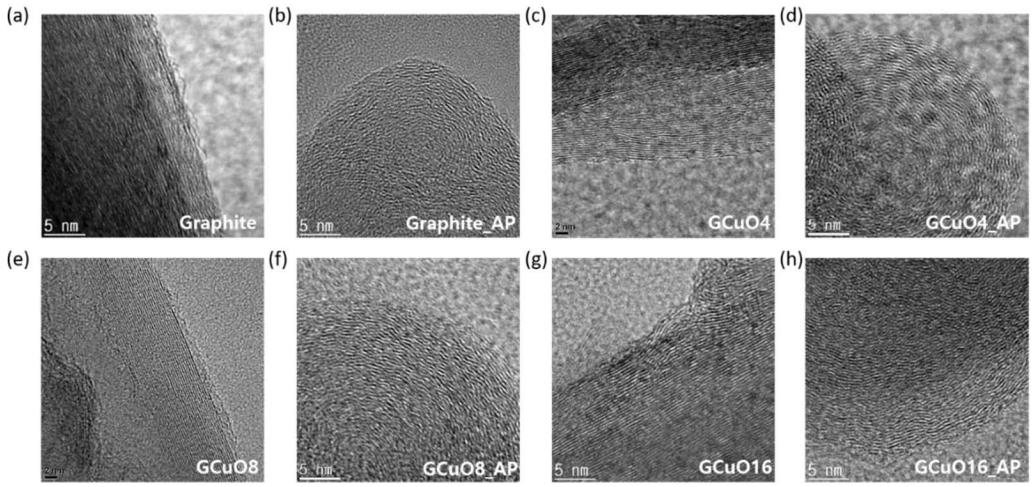

Figure 3.12 HR-TEM images of before pre-lithiation (a) Graphite, (c) GCuO4, (e) GCuO8, (g) GCuO16 and After pre-lithiation (b) Graphite, (d) GCuO4, (f) GCuO8, (h) GCuO16.

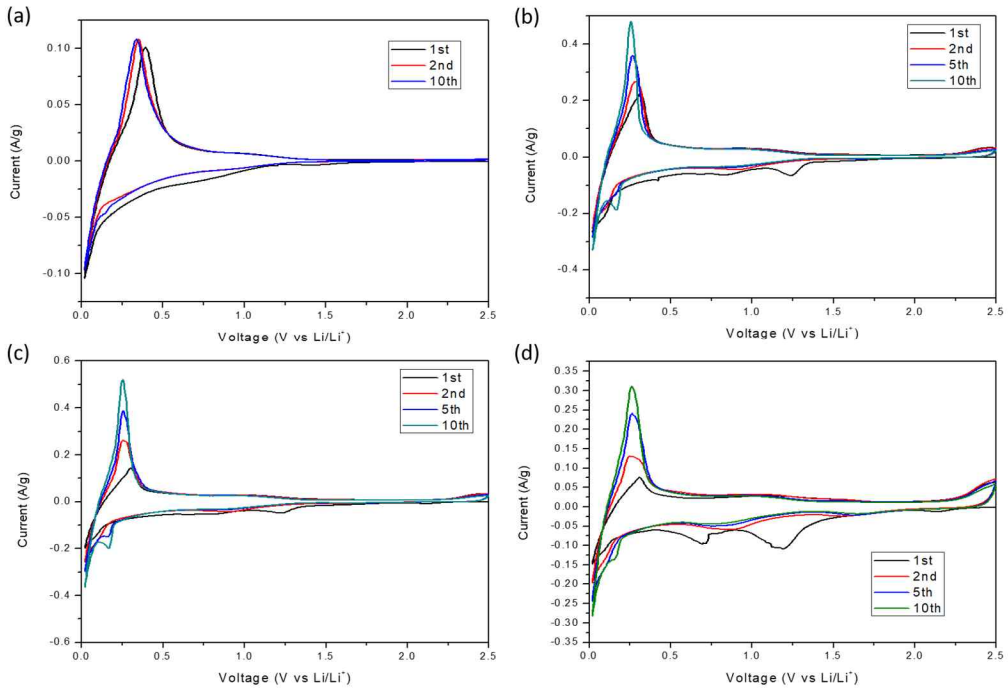

Figure 3.13 Repeated cyclo-voltammogram of (a) graphite, (b) GCuO4, (c) GCuO8 and (d) GCuO16 at 0.1 mV/s from 0.02 V to 2.5 V.

Table. 3.3 Weight fractions of copper oxide of GCuO4, GCuO8 and GCuO16.

	GCuO4	**GCuO8**	**GCuO16**
Weight fraction of copper oxide (%)	7.8	14.5	25.3

Chapter 4. Conclusion

We made a hybrid system with a high energy density similar to LIBs by using graphite/copper oxide composites (GCuO) and activated carbon (AC) as the negative electrode and the positive electrode, respectively. The proposed hybrid system employs both a faradaic intercalation/de-intercalation and conversion reaction of GCuO as well as a non-faradaic ion adsorption/desorption of AC. The hybrid system achieves a high energy density of 250 Wh kg^{-1} at 250 W kg^{-1} and 70Wh kg^{-1} at 12.5kW kg^{-1}. All processes were simple and cost effective. When the GCuOs are synthesized, the generated gas expands the interlayer spacing of the GCuOs so that the GCuOs have a low lithium insertion barrier. The optimum composition and the pre-lithiation conditions of the GCuO were verified. The pre-lithiation supplied Li source to the negative electrode led GCuO to have wider interlayer spacing and stable SEI layer. The prepared hybrid system shows excellent electrochemical performance in terms of the energy density and the power density when balancing between AC and GCuO kinetics due to the lowered internal resistance. It is more important to balance the kinetics between the negative and positive electrodes, although a high specific capacity negative electrode material is also important in a hybrid system. This research can be applied not only for hybrid capacitors like LICs, but also for various secondary batteries such as LIB and multivalent batteries. Consequently, they can provide inspiration for researchers in related fields.

Reference

[1] Cox, P.M., et al., Nature, 2000. **408**(6809): p. 184-187.

[2] Root, T.L., et al, Nature, 2003. **421**(6918): p. 57-60.

[3] Dresselhaus, M.S. and I.L. Thomas, Nature, 2001. **414**: p. 332.

[4] Panwar, N.L., S.C. Kaushik, and S. Kothari, Renewable & Sustainable Enrgy Reviews, 2011. **15**(3): p. 1513-1524.

[5] Schroeder, A. and T. Traber, Energy Policy, 2012. **43**: p. 136-144.

[6] Lu, L.G., et al., Journal of Power Sources, 2013. **226**: p. 272-288.

[7] Aravindan, V., et al., Chem Rev, 2014. **114**(23): p. 11619-35.

[8] Khomenko, V., E. Raymundo-Piñero, and F. Béguin, Journal of Power Sources, 2008. **177**(2): p. 643-651.

[9] Wang, H. and M. Yoshio, Journal of Power Sources, 2008. **177**(2): p. 681-684.

[10] Wang, H., et al Advanced Functional Materials, 2016. **26**(18): p. 3082-3093.

[11] Ajuria, J., et al., Journal of Power Sources, 2017. **363**: p. 422-427.

[12] Li, S., et al., Small, 2017. **13**(6).

[13] Lai, C.-M., T.-L. Kao, and H.-Y. Tuan, Journal of Power Sources, 2018. **379**: p. 261-269.

[14] Shin, D.H., et al., ACS Appl Mater Interfaces, 2014. **6**(5): p. 3312-9.

[15] Cho, S., et al., Journal of Materials Chemistry C, 2016. **4**(45): p. 10740-

10746.

[16] Cho, S., et al., Chemistry-A European Journal, 2017. **23**(48): p. 11629-11635.

[17] Lee, W.S.V., et al., ACS Appl Mater Interfaces, 2018. **10**(2): p. 1690-1700.

[18] Wang, B., et al., Journal of Materials Chemistry, 2010. **20**(47): p. 10661-10664.

[19] Wang, G.P., L. Zhang, and J.J. Zhang, Chemical Society Reviews, 2012. **41**(2): p. 797-828.

[20] Sivakkumar, S.R. and A.G. Pandolfo, Electrochimica Acta, 2012. **65**: p. 280-287.

[21] Zhang, J., Z. Shi, and C. Wang, Electrochimica Acta, 2014. **125**: p. 22-28.

[22] Jezowski, P., et al., Nat Mater, 2018. **17**(2): p. 167-173.

[23] Li, Y.M., L.H. Tang, and J.H. Li, Electrochemistry Communications, 2009. **11**(4): p. 846-849.

[24] Li, C., et al., Journal of Power Sources, 2010. **195**(9): p. 2939-2944.

[25] Sui, Y.M., et al., Crystal Growth & Design, 2010. **10**(1): p. 99-108.

[26] Ferrari, A.C., et al., Physical Review Letters, 2006. **97**(18).

[27] Gopiraman, M., et al., Acs Sustainable Chemistry & Engineering, 2015. **3**(10): p. 2478-2488.

[28] Podhajecky, P. and B. Scrosati, Journal of Power Sources, 1985. **16**(4): p. 309-317

[29] Zhou, J., et al., Electrochemistry Communications, 2011. **13**(12): p. 1357-

1360.

[30] Yin, Z., et al., Nano Research, 2017. **11**(2): p. 769-779.

[31] Cho, S.J., et al., Advanced Functional Materials, 2015. **25**(38): p. 6029-6040.

[32] Dees, D.W., et al., Journal of Power Sources, 2009. **189**(1): p. 263-268.

국 문 초 록

전기 자동차의 급격한 성장으로 인해 높은 용량의 에너지 저장 장치에 대한 관심이 높아지고 있다. 특히 전기자 산업에서 높은 에너지 밀도를 구현하기 위해서는 리튬 이온 전지가 가장 적합하다고 평가받고 있다. 그러나 리튬 이온 전지는 고유의 반응 메카니즘에 의해 느린 충전 속도를 가진다는 단점이 있다. 높은 출력 밀도를 유지하면서 높은 에너지 밀도를 가지는 하이브리드 형태의 리튬 이온 커패시터를 사용했다. 이 시스템은 흑연 구리 산화물을 음극으로 활성탄을 양극으로 구성되었다. 구리 산화물 합성은 구리 이온 복합체와 흑연에 열처리를 통해 이루어졌다. 구리 이온 복합체가 열적 분해가 일어나면서 발생하는 수소, 이산화탄소 기체가 발생하게 되고, 발생한 기체는 흑연의 간격을 팽창시킨다. 팽창된 흑연은 리튬의 삽입 장벽을 낮춘다. 동시에 높은 용량을 가진 구리 산화물이 흑연 표면에 생성된다. 위 특성을 지닌 흑연 구리 산화물은 높은 용량과 빠른 충방전이 가능하다. 따라서 하이브리드 시스템은 음극에서 흑연의 삽입 반응, 구리 산화물의 전환 반응을 이용하고, 양극에서는 활성탄과 전해질 사이의 전기 이중층에 의한 용량을 이용하여 전기에너지를 저장한다. 본 연구에서는 흑연과 구리 산화물의 비율, 전리튬화 조건을 조절하여 높은 에너지 밀도를 지니는 리튬 이온 커패시터를 구현했다. 최적화된 이 시스템은 250 W/kg의 출력 밀도에서 250 Wh/kg의 높은 에너지 밀도를 가지며, 이 값은 리튬 이온

전지의 에너지 밀도에 준한다. 10 kW/kg 의 출력 밀도에서도 70 Wh/kg의 에너지 밀도를 가진다.

주요어 : 리튬 이온 커패시터, 흑연층 간격, 리튬 이온 배터리, 슈퍼 커패시터, 전기 이중층, 전리튬화

학번 : 2017-26520